Chapter-3

QUASILINEAR ANALYSIS OF REGULAR PLASMA FIREBALL SHEATH INSTABILITY

Abstract: *One of the interesting instabilities excitable due to plasma-electrode interaction is plasma fireball sheath (PFBS) instability. The PFBS instability is analysed in this chapter in the framework of local quasilinear perturbation analysis in relevant laboratory scales. The perturbation analysis yields a second-order nonhomogeneous differential equation of variable coefficients. Which, upon solving with relevant boundary conditions, yields the general solution of the PFBS dynamics in terms of the spatially varying involved perturbed plasma parameters*[†]*. The peakonic profiles of the derived perturbed plasma parameters manifest the novelty of this PFBS analysis. These atypical theoretical results corroborate with the previously reported experimental outcomes. Finally, the applications of PFBS dynamics are highlighted at the end.*

3.1 INTRODUCTION

The laboratory plasma-electrode interaction has been a fascinating topic for the plasma physicists over the decades. Existence of extensive utilities of such plasma-wall effects in diversified cost-effective material-processing and manufacturing techniques is well-observed [1]. It inclines the plasma physics community more towards understanding the basic physics involved in the plasma-electrode (plasma-wall) interaction processes, instabilities, and so forth [2]. Besides, such interaction processes result in the formation of non-neutral space charge layers called plasma sheaths, separating the bulk plasma from the rest. The fireball (FB) glow is a special outcome of this plasma-electrode interaction.

The inter-constituent collisions across plasma trigger avalanche-like expansion of the plasma sheaths through ionisation. This expansion results in glowing structures, such as plasma fireballs (FBs). Such collisions lead to excitation of the neutral atoms. This excitation is responsible for the release of energy visible through the FB spectral glow [2]. The adjacent double layer (DL) outwards acts as a continuous source of charged particles developing the FB. The FB size relies on the rate of plasma production and of ion loss due to a modified electron–ion coupling [3]. Also, the adjacent DL plays an active role in varying the size of the sheath, and thus, the FB width in the process. Clearly, FBs are

[†]Dutta, S. and Karmakar, P. K. Fireball sheath instability. *J. Astrophys. Astron.*, 43(64):1-8, 2022.

discharge phenomena, formed mostly in low-temperature partially ionized plasmas. The regular FB (RFB) is formed in the sheath region around a solid electrode along with the formation of the DL outwards.

The plasma FB sheath (PFBS) has widespread practical realization across science, engineering, and technology [1]. The FB model evidently includes thermonuclear fusion plasmas, low-temperature plasmas, and plasma assisted technology on various laboratory and astrocosmic spatiotemporal scales [4, 5]. Besides, it helps in the formulation of high energy particle collision experiments generating quark-gluon plasma, especially the large hadron collider (LHC), relativistic heavy ion collider (RHIC), and super proton synchrotron (SPC). The FB geometry and its expansion pattern help in describing both the yields and the spectra of various particles experimented at the heavy ion synchrotron experiments, e.g., GSI SIS 18 in Germany and so forth [5]. Similarly, the study of inverted FBs [6] and the associated Buneman instabilities have significant importance in a good number of laboratory and astrophysical situations, such as stellar chromospheres [7], supernova (SN2011fe) explosion [8], cometary tails, bright meteoritic objects, ambient atmospheres, and so forth [9, 10]. The dynamic FB model also helps in explaining astronomical expansion of Gamma-ray bursts [11], as mentioned in Chapter-1.

The spatiotemporal nature of the PFBS is extensively evident in both laboratory [3, 12] as well in astrocosmic scales [10]. A theoretical model to explore the saturation mechanisms thereof is yet to be developed to the best of our knowledge. It forms the main motivational force for this semi-analytic PFBS analysis in a bifluidic fabric. The existent plasma components, i.e., electrons and ions are considered as two sperate individual fluids. The plasma medium with these two separate fluids is categorised as bifluidic plasma. A quasilinear perturbation turns the PFBS system into a unique class of second-order ordinary differential equation (ODE) on the perturbed electrostatic potential with variable coefficients. A numerical integration results in peakon-type structures and so forth.

3.2 PHYSICAL MODEL AND FORMALISM

We consider the PFBS formation around a solid anode of spherical geometry (as in Fig. 1.1(a)) submerged in a bifluidic plasma. The proposed model consists mainly of electronic and ionic fluids with a negligible role of neutral component(s). It is obviously consistent and correlative with the plasmas well-realisable in laboratories. It may be noted herein that the experimental observations of plasma FBs show a consistently spherical geometric shape in such circumstances [2]. The consideration of the spherically symmetric geometry

reduces the complex 3-D spherical problem into a simple 1-D radial problem without violating any kind of dynamical reality irrespective of spatiotemporal scales [13]. The full dynamics of the electronic and ionic fluids are governed by their respective electrodynamic governing equations evolving on their relevant laboratory spatiotemporal scales fulfilling the plasma existential conditions $((r,t) >> (\lambda_D, \omega_p^{-1}))$. The model closure is obtained with the help of coupling electrostatic Poisson equation describing the potential distribution developed due to local charge imbalance. At the beginning, the bulk macroscopic state of the entire plasma distribution forms a quasineutral hydrostatic homogeneous equilibrium.

It should relevantly be noted that both plasma FBs and related sheath are experimentally observed to undergo diverse spatiotemporal fluctuations. The spatiotemporal fluctuation primarily occurs in terms of electrostatic potential across it, current passing through it, and discharge light emanated from it [2], etc. In our analysis, we consider only the asymptotic steady-state plasma fluctuations for the sake of simplifying the mathematical analysis against the initial state. Thus, it hereby enables us to transform our theoretic formalism to a steady-state model ansatz (time-stationary), but with no inherent loss of any kind of generality in the PFBS evolution.

We are now, motivated to see a quasilinear FB sheath-plasma instability within the valid framework of a local perturbation analysis against the equilibrium. The corresponding basic governing equations describing the classical nonrelativistic dynamics of the PFBS structure evolution with all the generic plasma notations [14] in a spherically symmetric coordination space (r, t) are respectively enlisted as

$$\frac{\partial n_e}{\partial t} + \left(\frac{1}{r^2}\right)\frac{\partial}{\partial r}(r^2 n_e v_e) = 0, \tag{3.1}$$

$$m_e n_e \frac{\partial v_e}{\partial t} + m_e n_e v_e \frac{\partial v_e}{\partial r} = n_e e \frac{\partial \phi}{\partial r} - T_e \frac{\partial n_e}{\partial r}, \tag{3.2}$$

$$\frac{\partial n_i}{\partial t} + \left(\frac{1}{r^2}\right)\frac{\partial}{\partial r}(r^2 n_i v_i) = 0, \tag{3.3}$$

$$m_i n_i \frac{\partial v_i}{\partial t} + m_i n_i v_i \frac{\partial v_i}{\partial r} = n_i e \frac{\partial \phi}{\partial r} - T_i \frac{\partial n_i}{\partial r}. \tag{3.4}$$

Here, $n_{e(i)}$, $v_{e(i)}$, $m_{e(i)}$, and $T_{e(i)}$ denote the population density, flow velocity, mass, and temperature of electron (ion), respectively.

It is to be noted here that Eqs. (3.1)-(3.2) represent the equation of continuity and that of momentum for the electronic dynamics. Similarly, Eqs. (3.3)-(3.4) depict the same

for the ions. The electron-ion closure electrostatic Poisson equation in the spherically symmetric geometry reads as

$$\frac{1}{r^2}\frac{\partial}{\partial r}\left(r^2\frac{\partial \phi}{\partial r}\right) = 4\pi e(n_e - n_i). \tag{3.5}$$

Here, ϕ is the electrostatic potential developed due to local charge imbalance. The electron (ion) charge $e = 1.9 \times 10^{-19}$ C is the quantized unit of charge magnitude of the ionic constituents in plasma. Clearly, it is revealed physically from Eq. (3.5) that electric polarization effects (charge separation) always result in a commensurable electrostatic potential (or field) distribution in the coordination space irrespective of time scales. So, the left-hand side of Eq. (3.5) is always independent of time, even if the charge distribution in the right-hand side in isolation is not. It justifies the analytic nature of Eq. (3.5).

We are interested in the steady-state evolution of the PFBS fluctuations ($\partial/\partial t \sim 0$, but $\partial/\partial \xi \neq 0$) in the considered spherical geometry. We adopt here a standard normalization scheme well validated for laboratory plasmas [15]. Accordingly, the normalized forms of Eqs. (3.1)-(3.4) are obtained in the time-stationary (steady-state) shape respectively cast as

$$M_e\ \frac{\partial N_e}{\partial \xi} + N_e\frac{\partial M_e}{\partial \xi} + \left(\frac{2}{\xi}\right)M_eN_e = 0, \tag{3.6}$$

$$N_e\ \frac{\partial \Phi}{\partial \xi} = N_eM_e\left(\frac{m_e}{m_i}\right)\frac{\partial M_e}{\partial \xi} + \frac{\partial N_e}{\partial \xi}, \tag{3.7}$$

$$M_i\frac{\partial N_i}{\partial \xi} + N_i\frac{\partial M_i}{\partial \xi} + \left(\frac{2}{\xi}\right)M_iN_i = 0, \tag{3.8}$$

$$N_i\ \frac{\partial \Phi}{\partial \xi} = N_iM_i\frac{\partial M_i}{\partial \xi} + \left(\frac{T_i}{T_e}\right)\frac{\partial N_i}{\partial \xi}. \tag{3.9}$$

The electrostatic Poisson equation (Eq. (3.5)) in the normalized form is similarly cast as

$$\frac{\partial^2 \Phi}{\partial \xi^2} + \left(\frac{2}{\xi}\right)\frac{\partial \Phi}{\partial \xi} = N_e - N_i. \tag{3.10}$$

The normalized radial distance is given as $\xi = r/\lambda_D$; where, $\lambda_D = \sqrt{T_e/4\pi ne^2}$ is the plasma Debye length. The normalized electron (ion) population density is $N_{e(i)} = n_{e(i)}/n_{e(o)} = n_{e(i)}/n_o$; where, n_o is the equilibrium density. The electronic (ionic) fluid

Mach number is $M_{e(i)} = v_{e(i)}/c_s$; where, $c_s = \sqrt{T_e/m_i}$ is the ion-sound phase speed. $\Phi = \mathrm{e}\phi/\mathrm{T_e}$ is electrostatic potential normalized to the electron thermal potential, T_e/e.

The diverse relevant physical variables ($F_\alpha(\xi)$) in Eqs. (3.6)-(3.10) now undergo a quasilinear local perturbation against their respective equilibrium values (F_o) on the ϵ-order expansively as presented below

$$F(\xi) = F_o + \sum_{\alpha=1}^{\infty} \epsilon^\alpha F_\alpha(\xi). \tag{3.11}$$

Here, ϵ is an order parameter signifying the balanced strength of nonlinearity and dispersion [15]. An order-by-order analysis with Eq. (3.11) put in Eqs. (3.6)-(3.9) up to the first-order yields

$$\frac{\partial M_{e1}}{\partial \xi} + \left(\frac{2}{\xi}\right) M_{e1} = 0, \tag{3.12}$$

$$\frac{\partial \Phi_1}{\partial \xi} = \frac{\partial N_{e1}}{\partial \xi}, \tag{3.13}$$

$$\frac{\partial M_{i1}}{\partial \xi} + \left(\frac{2}{\xi}\right) M_{i1} = 0, \tag{3.14}$$

$$\frac{\partial \Phi_1}{\partial \xi} = \left(\frac{T_i}{T_e}\right) \frac{\partial N_{i1}}{\partial \xi}. \tag{3.15}$$

After an indefinite ξ-integration on Eqs. (3.12)-(3.15) with the relevant boundary conditions (at $\xi = 0, \infty$) usually realizable in laboratory plasmas, we get the solutions of these equations respectively given as

$$M_{e1} = \frac{c_{eM}}{\xi^2}, \tag{3.16}$$

$$N_{e1} = \Phi_1 + c_{eN}, \tag{3.17}$$

$$M_{i1} = \frac{c_{iM}}{\xi^2}, \tag{3.18}$$

$$N_{i1} = \theta_{ei}\Phi_1 + c_{iN}. \tag{3.19}$$

Here, c_{eM}, c_{eN}, c_{iM}, and c_{iN} are integration constants, which could be determined with the application of appropriate boundary conditions of the problem without loss of any generality. The electron-to-ion temperature ratio is $\theta_{ei} = T_e/T_i$. Replacement of N_{e1} and N_{i1} from respective Eq. (3.17) and Eq. (3.19) in the first-order quasilinearly perturbed form of Eq. (3.10) gives an ODE cast as

$$\frac{\partial^2\Phi_1}{\partial\xi^2}+\left(\frac{2}{\xi}\right)\frac{\partial\Phi_1}{\partial\xi}=\Phi_1(1-\theta_{ei})-(c_{eN}-c_{iN}). \tag{3.20}$$

Through multiplying ξ^2 with Eq. (3.20), it may be transformed as

$$\xi^2\frac{\partial^2\Phi_1}{\partial\xi^2}+2\xi\frac{\partial\Phi_1}{\partial\xi}=\xi^2\Phi_1(1-\theta_{ei})-\xi^2(c_{eN}-c_{iN}). \tag{3.21}$$

The term, $(1-\theta_{ei})$ in Eqs. (3.20)-(3.21) physically denotes the deviation of the fireball-sheath region from the isothermal condition. The analytic solution of Eq. (3.20), with the usual set of realistic boundary conditions [16], manifests the evolution of the perturbed electrostatic potential in the PFBS region. An integration of Eq. (3.20) yields

$$\Phi_1(\xi)=\frac{(1-(\sqrt{-c_1})\xi)c_2}{2(-c_1)^{\frac{3}{2}}\xi}-\frac{(1+(\sqrt{-c_1})\xi)c_2}{2(-c_1)^{\frac{3}{2}}\xi}+\frac{\exp\left((\sqrt{-c_1})\xi\right)c_3}{\xi}-\frac{\exp(-(\sqrt{-c_1})\xi)c_4}{2(\sqrt{-c_1})\xi}. \tag{3.22}$$

Here, $c_1=\theta_{ei}-1$, $c_2=c_{eN}-c_{iN}$. c_3 and c_4 are the integration constants to be evaluated on the grounds of imposition of appropriate boundary conditions in conformity with bolstering experimental findings [1]. The constant $c_2=(c_{eN}-c_{iN})$, denotes the population density difference of the electrons and ions at a very large distance from the plasma sheath or the FB. Here, the electrostatic potential due to the embedded electrode is not experienced. The constant c_3 denotes the electrostatic potential value at unit Debye length (Eq. (3.28)).

In nonthermal plasmas, $\theta_{ei}\geq 1$; so, one gets, $\sqrt{-c_1}=\sqrt{(1-\theta_{ei})}=i\sqrt{c_1}$. So, Eq. (3.22) reads

$$\Phi_1(\xi)=\frac{(1-(i\sqrt{c_1})\xi)c_2}{2(-c_1)^{\frac{3}{2}}\xi}-\frac{(1+(i\sqrt{c_1})\xi)c_2}{2(-c_1)^{\frac{3}{2}}\xi}+\frac{\exp\left((i\sqrt{c_1})\xi\right)c_3}{\xi}-\frac{\exp(-(i\sqrt{c_1})\xi)c_4}{2(i\sqrt{c_1})\xi}. \tag{3.23}$$

A simplified form of Eq. (3.23) can be given as

$$\Phi_1(\xi)=\frac{c_2}{c_1}+\frac{\exp\left((i\sqrt{c_1})\xi\right)c_3}{\xi}-\frac{\exp(-(i\sqrt{c_1})\xi)c_4}{2(i\sqrt{c_1})\xi}. \tag{3.24}$$

It is noteworthy that the terms involving $1/\xi$, appears above because of spherical geometry, which would, otherwise, be absent on the grounds of planar geometry [17, 18]. We are interested in the localized potential solutions around our reference point, $\xi \approx 0$. Application of the small amplitude approximation in Eq. (3.24) gives

$$\Phi_1(\xi) = \frac{c_2}{c_1} + \frac{c_3}{\xi}[1 + i\sqrt{c_1}\,\xi + \frac{1}{2!}(i\sqrt{c_1})^2\xi^2 + \frac{1}{3!}(i\sqrt{c_1})^3\xi^3 + \frac{1}{4!}(i\sqrt{c_1})^4\xi^4 + \cdots)] - \frac{c_4}{2(i\sqrt{c_1})\xi}[1 + (-i\sqrt{c_1})\xi + \frac{1}{2!}(-i\sqrt{c_1})^2\xi^2) + \frac{1}{3!}(-i\sqrt{c_1})^3\xi^3 + \frac{1}{4!}(-i\sqrt{c_1})^4\xi^4 - \cdots]. \quad (3.25)$$

Eq. (3.25) can also be rearranged in terms of real and imaginary terms as

$$\Phi_1(\xi) = \frac{c_2}{c_1} + \frac{c_3}{\xi}[(1 - \frac{1}{2!}c_1\xi^2 + \cdots) + i(\sqrt{c_1}\,\xi - \frac{1}{3!}(c_1)^{\frac{3}{2}}\xi^3 + \cdots)] + \frac{c_4}{2\xi}[(\xi + \frac{1}{3!}c_1\xi^3 - \cdots) - i((\sqrt{c_1})^{-1} - \frac{1}{2!}\sqrt{c_1}\xi^2 + \cdots)]. \quad (3.26)$$

A comparison of the real and imaginary terms from both the left and the right-hand sides of Eq. (3.26) yields the actual perturbed electrostatic potential as

$$\Phi_1(\xi) = \frac{c_2}{c_1} + \frac{c_3}{\xi}\left(1 - \frac{1}{2!}c_1\xi^2 + \frac{1}{4!}{c_1}^2\xi^4 - \cdots\right) + \frac{c_4}{2\xi}\left(\xi - \frac{1}{3!}c_1\xi^3 + \frac{1}{5!}{c_1}^3\xi^5 - \cdots\right). \quad (3.27)$$

It may be seen that Eq. (3.27) is analogous to the common Fourier series expansion of any arbitrary signal [18]. In that Fourier perspective, the first free term, c_2/c_1 on the right-hand side would represent the zero-frequency line. The coefficient term, c_3/ξ, would denote the even harmonic strength. Similarly, the last coefficient term, $c_4/2\xi$, would designate the strength of odd harmonicity in the expansion series.

Using the physically sensible boundary conditions ($\Phi_1(\xi \to \pm\infty) \to 0$), Eq. (3.27) yields

$$\Phi_1(\xi) = \frac{c_3}{\xi}. \quad (3.28)$$

It may be noteworthy that, c_3 in Eq. (3.28) could physically also signify the relative strength of the electrostatic potential in the intervening plasma. Now, due to our interest in the

positive amplitude solutions of the locally perturbed electrostatic potential structures in full consistency with the literature [1], Eq. (3.28) gets, therefore, amended to

$$\Phi_1(\xi) = \frac{c_3}{|\xi|}. \tag{3.29}$$

The corresponding perturbed electric field, that is obtained from Eq. (3.28) using the universal law of conservative force field, can be presented as follows

$$\mathrm{E}_1(\xi) = -\frac{\partial \Phi_1}{\partial \xi} = \frac{c_3}{\xi^2}. \tag{3.30}$$

The above analytic field expression, $E_1(\xi) = c_3/\xi^2$, can also be derived from the electrostatic potential, $\Phi_1(\xi) = c_3/\xi$, via a calculus limit theorem defined by the first principle as: $E_1 = -\underset{\xi_2 \to \xi_1}{Lt}[\Phi_1(\xi_2) - \Phi_1(\xi_1)]/(\xi_2 - \xi_1) = \underset{\xi_2 \to \xi_1}{Lt}[(c_3/\xi_1 - c_3/\xi_2)]/(\xi_2 - \xi_1) = c_3/\xi_2^2 = c_3/\xi^2$ for $\xi = \xi_2$. It could directly be used to examine the validity of the field-potential profile evolutionary mapping as elaborately discussed later.

A detailed numerical illustrative platform is developed to see the evolution of the potential perturbation in the form of spatial potential profiles ($\Phi_1 = \Phi_1(\xi)$, Fig. 3.1(a)), spatial field profiles ($\mathrm{E}_1 = \mathrm{E}_1(\xi)$, Fig. 3.1(b)), and conjoint colormaps with the help of a triangular coupling of Eq. (3.29) and Eq. (3.30) via ξ ($\mathrm{E}_1 = \mathrm{E}_1(\xi, \Phi_1)$, Fig. 3.2). The different colormaps link to the different c_3-values (as indicated).

3.3 RESULTS AND DISCUSSIONS

A theoretical bifluidic model is constructed herein to study the quasilinear PFBS instability dynamics in the relevant laboratory scale. The quasilinearity arises because of a weak coupling between the nonlinear fluid convection and linear fluid dispersion (via ϵ). Application of the quasilinear perturbative analysis reduces the PFBS system into a unique construct of a linear second-order ODE having a unique set of variable multiparametric coefficients (Eqs. (3.20)-(3.21)). The first-order perturbed electrostatic potential and the corresponding electric field are analytically evaluated and numerically portrayed in realistic plasma parametric windows. It is fairly supported by both the theoretical boundary conditions [16] and the experimental PFBS observations [1].

The peakonic pulse potential structures semi-analytically observed herein signify the saturation undergoing in the PFBS instability (Fig. 3.1(a)). The associated narrow peakon fields are to be analysed from a dispersive conservative force field perspective (Fig. 3.1(b)). A quicker reliability validation of Fig. 3.1(b) may be instantly drawn by using the limiting graphical analysis in the light of Fig. 3.1(a). It is seen that (Fig. 3.1(a)), $\Phi_1(\xi = -0.5) = 5$ and $\Phi_1(\xi = -0.6) = 4$; yields $E_1 = [(\Phi_1(\xi = -0.5) - \Phi_1(\xi = -0.6)]/[-0.5 - (-0.6)] = 10$ (as in Fig. 3.1(b)). Simultaneously, one finds that $E_1(\xi = -0.55)=10$ graphically (Fig. 3.1(b)), which is same as above. It validates the reliability of our entire calculation scheme via Fig. 3.1(b) as an outcome of Fig. 3.1(a).

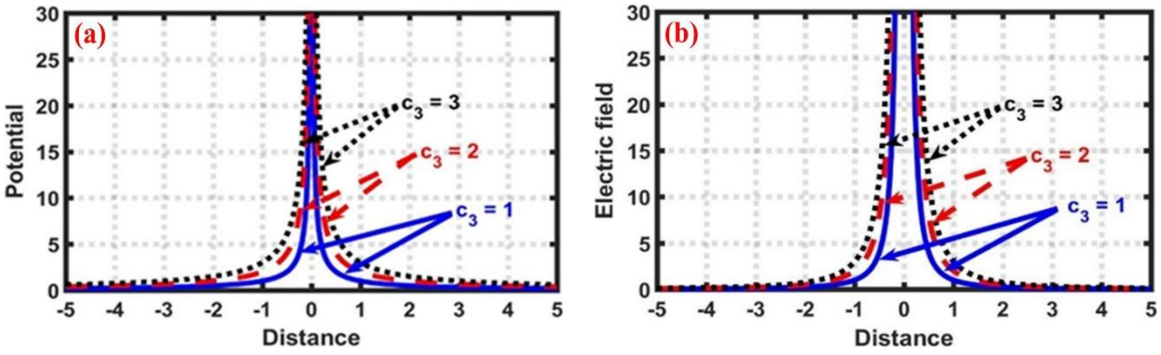

Figure 3.1*: Profile of the perturbed normalized (a) electrostatic potential ($\Phi_1 = f(\xi)$), governed by Eq. (3.24)) and (b) electric field ($E_1 = -\partial\Phi_1/\partial\xi$), governed by Eq. (3.25)) with variation in the normalized radial distance relative to the electrode surface.*

In Fig. 3.2, the different lines link to the potential strength arising for $c_3 = 1$ (blue solid line), $c_3 = 2$ (red dashed line), and $c_3 = 3$ (black dotted line). The peakon-type structures peak at the origin of the spherical coordinate system.

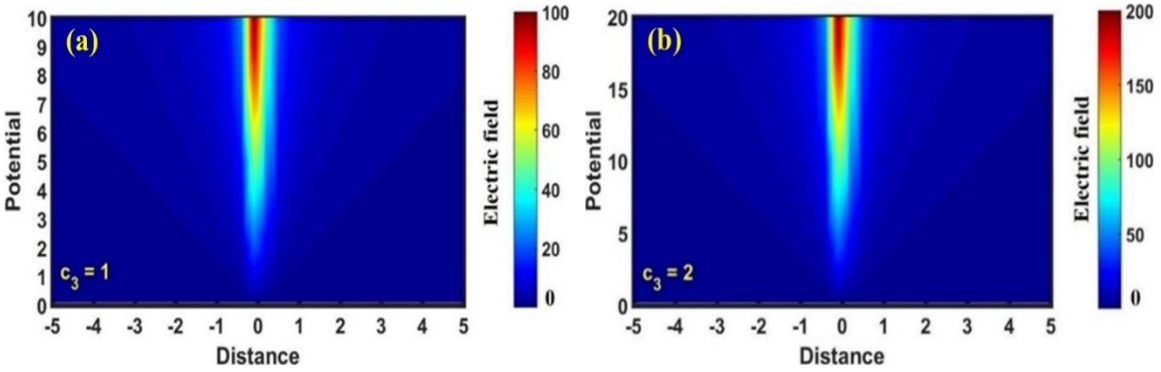

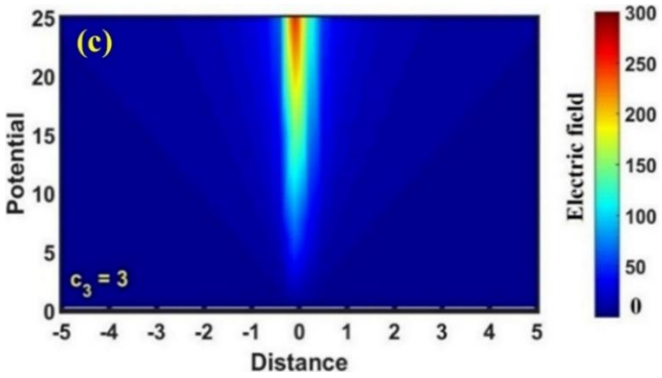

***Figure 3.2**: Colormap showing the evolution of the perturbed normalized electrostatic potential (Φ_1) and the corresponding electric field (E_1) with variation in the normalized radial distance (ξ).*

The different maps in Fig. 3.2 (viz., (a), (b), and (c)) correspond to $c_3 = 1$, 2, and 3, respectively. A sharp color change at the center hints at a greater rate of the (Φ_1, E_1)-variation. The out-fading color replicates a meagre (Φ_1, E_1)-change off-centrally.

The Fig. 3.2 manifests the collective spatial variation of the potential (Φ_1) and electric field (E_1) in terms of the colour density and gradient in accordance with Figs. 3.1(a)-3.1(b). Thus, the previous patterns (Figs. 3.1(a)-3.1(b)) of the steady-state instability evolution are fairly confirmed by the colour spectral profiles (Fig. 3.1(b)). In addition to the above, a spatially fast variation of the surface colour around the reference point characterises a faster rate of the E_1-variation. In contrast, a slower colour spectral variation asymptotically indicates a weaker change in E_1 from the reference point outwards. Thus, the steady saturation of the instability in the proposed plasma model configuration is graphically confirmed. It may be pertinent to add here that the reliability of the spherically symmetric FB model analysis is further strengthened in light of the qualitative matching of our obtained results (Figs. 3.1-3.2) with the available experimental [1, 13] and theoretical [6] findings reported extensively in the literature.

3.4 CONCLUSIONS

The steady PFBS dynamics excited around a RFB of spherical geometry is analysed herein theoretically in a bifluidic plasma model framework. An applied quasilinear perturbative analysis (relative to a well-defined hydrostatic homogeneous equilibrium) reduces the perturbed PFBS system under test into a unique construct of a second-order linear ODE with variable coefficients. The formation of peakon-type potential and electric field

structures around the electrode is numerically investigated. The peakonic features are confirmed in colourspectral phase space as well. It is shown that peakonic structures could result even from a linear ODE system against the traditional peakonic picture of fully nonlinear dynamical systems [17, 18]. The representation of peakon structures herewith the exponential functions is quite in agreement with the earlier predictions reported in the literature [17, 18]. As a consequence, it may be fairly conjectured that our analysis provides a theoretical platform to support the experimentally observed PFBS potential structures from the bifluidic perspective. The atypical eigen-patterns are fairly consistent and correlative with experimental findings reported elsewhere [1]. Thus, our analysis could be additionally applicable to understand the coupling stability scenarios of plasma sheath, FB, and double layer on the usual laboratory scales.

It may be added here that the fully nonlinear systems manifest peakons of the form $\exp\{-(r-vt)/L\}$; here, r, v, t and L denote the radial distance of observation from system centre, velocity of the peakon, time of observation, and soliton length, respectively [16]. Whereas weakly nonlinear (quasilinear) asymptotic systems (as analysed herein) are observed to manifest atypical peakonic profiles of the form $1/r^n$, with $n \geq 1$.

Inclusion of magnetic field, external electric field, and non-spherical fireball geometry can deviate a linear or quasilinear system from the exponential peakonic form.

The PFBS instability dynamics and the FB model may find its application in various plasma processing systems alongside sheath-induced astrolabplasmic circumstances of great applied value. In a broader sense, the plasma FBs exert substantial pressure on the neutral and ionic components; thereby, inducing a macroscopic bulk gaseous flow in the test space-plasma medium taken under consideration, resulting in a plasma-jet phenomenon. As a result, a fair understanding of the plasma FBs and instabilities could enable us in developing a low-cost jet propulsion device for space-based technical explorations [19]. A comprehensive plasma concept of various associated instabilities is still in infancy stage as far as seen. It is believed that this analysis could be a promising element for illuminating this important direction having both laboratory and astrophysical plasma significances in future.

REFERENCES

[1] Stenzel, R. L., Gruenwald, J., Ionita, C., Scrittwieser, R. an Urrutia, J. M., Sheaths and double layers with instabilities. *J. Technol. Space Plasmas*, 2(1):70-91, 2021.

[2] Stenzel, R. L., Ionita, C., and Schrittwieser, R. Dynamics of fireballs. *Plasma Sources Sci. Technol*., 29(5):053001(1-11), 2008.

[3] Stenzel, R. L., Gruenwald, J., Fonda, B., Ionita, C. and Schrittwieser, R. Transit time instabilities in an inverted fireball, I. Basic properties. *Physics of Plasmas*, 18 (1):012104(1-9), 2011.

[4] Bandara, R. and Khachan, J. Nonlinear saturation of the ion-electron Buneman instability in a spherical positively pulsed gridded inertial electrostatic confinement device. *Phys. Plasmas*, 22(8):082701(1-12), 2015.

[5] Gruenwald, J., Reynvaan, J., and Knoll, P. Creation and characterization of inverted fireballs in H_2 plasma. *Phys. Scr*. T61(1):014006(1-3), 2014.

[6] Gruenwald, J., Reynvaan, J., and Knoll, P. Creation and characterization of inverted fireballs in H_2 plasma. *Phys. Scr*. T61(1):014006(1-3), 2014.

[7] Harabasz, S., Florkowski, W., Galatyuk, T., Gumberidze, M., Ryblewski, R., Salabura, P., Stroth, J. Thermal model description of the particle spectra in the few-GeV energy regime, *EPJ Web of Conferences*, 259(11008):1-4, 2022.

[8] Fontenla, J. M., Peterson, W. K., and Harder, J. Chromospheric heating by the Farley-Buneman instability, *Astron. Astrophys*, 480(3):839-846, 2008.

[9] Dessart, L., Blondin, S., Hiller, D. J. and Khokhlov, A. Constraints on the explosion mechanism and progenitors of Type Ia supernovae. *MNRAS*, 441(1):532-550, 2014.

[10] https://www.imo.net/definitions-of-terms-in-meteorastronomy-iau/

[11] Meng, Y-Z., Geng, J-J. and Wu, X-F. The photosphere emission spectrum of hybrid relativistic outflow for gamma -ray bursts. *MNRAS*, 509(4):6047-6058, 2022.

[12] Bariselli F., Frezzotti A., Hubin A. and Magin, T. E. Aerothermodynamic modelling of meteor entry flows. *MNRAS*, 492(2):2308-2325, 2020.

[13] Stenzel, R. L. Instability of sheath plasma resonance. *Phys. Rev. Lett*., 60(8):704-707, 1988.

[14] Siemens, P. J. and Rasmussen, J. O. Evidence for a blast wave from compressed nuclear matter, *Phys. Rev. Lett*. 42(14):880-883, 1979.

[15] Gohain, M. and Karmakar, P. K. A generalized two-fluid model of plasma sheath equilibrium structure. *EPL*, 112(4):45002(1-6), 2015.

[16] Chen, F. F. *Introduction of Plasma Physics and Controlled Fusion*. Plenum Press, New York, 1984.

[17] Degasperis, A. Holm, D. D. Hone, A. N. W. A new integrable equation with peakon solutions. *Theor. Math. Phys*., 133(2):1463-1474, 2002.

[18] Holm, D. D. and Hone, N. W. A class of equations with peakon and pulson solutions. *J. Nonlin. Math. Phys.*, 12(1):380-394, 2005.

[19] Gruenwald, J., Kovacic, J., Fonda. B. and Gyergyek, T. A model for the basic plasma parameter profiles and the force exerted by fireballs with non-isothermal electrons. *Phys. Plasmas*, 25(113508):1-7, 2018.